Computers and Geotechnics xxx (2017) xxx–xxx

Contents lists available at ScienceDirect

Computers and Geotechnics

journal homepage: www.elsevier.com/locate/compgeo

Research Paper

Development of coupled numerical model for simulation of multiphase soil

K. Edip [a,*], V. Sesov [a], C. Butenweg [b], J. Bojadjieva [a]

[a] Institute of Earthquake Engineering and Engineering Seismology, Skopje, Macedonia
[b] Applied Mechanics and Structural Engineering, FH Aachen, Jülich 52428, Germany

ARTICLE INFO

Article history:
Received 28 January 2017
Received in revised form 10 August 2017
Accepted 28 August 2017
Available online xxxx

Keywords:
Coupled soil-water-air model
Finite element analysis
Hypoplasticity

ABSTRACT

In this paper, a coupled multiphase model considering both non-linearities of water retention curves and solid state modeling is proposed. The solid displacements and the pressures of both water and air phases are unknowns of the proposed model. The finite element method is used to solve the governing differential equations. The proposed method is demonstrated through simulation of seepage test and partially consolidation problem. Then, implementation of the model is done by using hypoplasticity for the solid phase and analyzing the fully saturated triaxial experiments. In integration of the constitutive law error controlling is improved and comparisons done accordingly. In this work, the advantages and limitations of the numerical model are discussed.

1. Introduction

Soil as a porous medium is composed of a solid skeleton and pores, which are filled with water and/or air. In describing porous media, it is important to consider the interaction between solid, water and air phases. This interaction among the phases is particularly important in dynamic conditions such as cyclic loading. Modeling based on the porous media theory in which an average macroscopic continuum is considered has proved to be useful to better understand coupled phenomena such as flow and deformation processes. An important contribution of the paper is that it demonstrates that the numerical framework is able to consider non linearities in simulation of both flow and deformation.

Modern formulations based on multiphase mixture theories were developed in the last decade as described in details in the monograph of de Boer [1]. In order to present an introductory review of the developed theories, the Terzaghi theory can be referred as the first study of deformable porous media which dealt with the one-dimensional consolidation theory on the basis of the effective stress concept [2]. In the works of Biot [3,4] the one-dimensional theory was extended to a three-dimensional theory of consolidation. Modern mixture theories were developed based on the concept of volume fractions by Morland [5], Goodman and Cowin [6], Sampaio [7] and Bowen [8,9]. Averaging theories were developed by Whitaker [10,11] and Hassanizadeh and Gary [12–14]. The work of Biot was extended to three phase conditions with a pore air as the third phase by Fredlund and Morgenstern [15] and Chang and Duncan [16]. The theory was developed by de Boer and Kowalski [17] on material non linearity behavior of the soil skeleton in the Terzaghi Biot framework. A simple extension of the two-phase formulation of porous media considering the air pressure to be constant and equal to the atmospheric pressure was proposed by Zienkiewicz et al. [18].

A generalized incremental form which includes large deformation and nonlinear material behavior was derived by Zienkiewicz et al. [19] for liquefaction analysis of soil structures. Coupled formulations that involve both air and water phases in soils were proposed by Alonso et al. [20], Schrefler et al. [21] and Gawin et al. [22]. A general reference for the use of finite element method for the numerical simulation of fluid flow and deformation processes in porous media is the monograph by Lewis and Schrefler [23]. Recent contributions to this topic include the one in Schrefler and Scotta [24] where a two-phase flow model is used leading to two pressure variables in addition to the displacement field to be approximated by suitable finite element spaces.

The most computational aspects of coupled finite elements have been presented in both linear and nonlinearly elastic material law for fluid saturated porous solids. Wieners et al. [25] in their work consider saturated porous medium flow where the material behavior of the porous skeleton is assumed to be elasto viscoplastic. Most recently, in the work of Oettl [26] a coupled multiphase formulation is applied to geotechnical problems considering different water retention relations. The work of Holler [27] follows the

* Corresponding author.
E-mail address: kemal@pluto.iziis.ukim.edu.mk (K. Edip).

https://doi.org/10.1016/j.compgeo.2017.08.016
0266-352X/

Oettl's work in which different material models for solid phase including hypoplasticity is considered. In this particular work the development of a coupled multiphase model follows the model of Holler [27].

The model is validated against the seepage experiment of Liakopoulos [28] and partially consolidated column as given in the work of Khoei and Mohammadnejad [29]. Finally, the multiphase model is considered in the simulation of triaxial element tests in both static and dynamic conditions.

The main purpose of this paper is to present a more realistic coupled model with hypoplastic modeling of the solid state behavior of saturated and/or unsaturated soils. As for notations and symbols used in this paper, bold faced letters denote tensors and vectors; the symbol '.' denotes an inner product of two vectors (e.g. $\mathbf{a}\cdot\mathbf{b} = a_i b_i$), or a single contraction of adjacent indices of two tensors (e.g. $\mathbf{c}\cdot\mathbf{d} = c_{ij}d_{jk}$); and the symbol ':' denotes an innerproduct of two second-order tensors (e.g. $\mathbf{c}:\mathbf{d} = c_{ij}d_{ij}$), or a double contraction of adjacent indices of tensors of rank two and higher (e.g. $\mathbf{C}:\boldsymbol{\varepsilon}^e = C_{ijkl}\varepsilon^e_{kl}$).

2. Formulation of coupled numerical model

The numerical model containing unsaturated, or in simpler form saturated deformable porous media behavior is based on the Theory of Porous Media (TPM). This approach can be described by use of the macroscopic continuum approach proceeding from the classical theory of mixtures with additional use of the volume fraction concept. The fundamentals of porous media theories, the development and comparison with other approaches to multiphase materials can be taken from literature. The interested reader is referred to the articles by de Bowen and Ray [8,9], Bedford and Drumheller [30], de Boer and Ehlers [31], Volk and Ehlers [32] and Ricken and de Boer [33].

In porous media, the mechanical behavior of deformable porous media and the interaction among phases are considered through mass conservation, equilibrium and from the solid skeleton's constitutive behavior. In this contribution, the soil medium is considered as a porous medium composed of solid, water and air phases. Pressures of water and air phases (p_w and p_a) and displacement in two directions u_x and u_y of the solid skeleton are taken as independent variables. Local thermodynamic equilibrium is assumed and temperature is kept constant through the analyzed domain. The first quantity that is derived is the capillary pressure, which is obtained as a water to air pressure difference. Namely,

$$p_c = p_a - p_w \tag{1}$$

In partially saturated state the voids in the porous medium are filled partly by water and air. The sum of respective degrees of saturation for water saturation S_w and air saturation S_a is one:

$$S_w + S_a = 1 \tag{2}$$

Once the capillary pressure and saturation relations are known the relations between water and air saturations are evaluated by means of experimentally determined functions such as:

$$S_w = 1 - S_a = S_w(p_c) \tag{3}$$

The constitutive law of the solid phase is written in terms of the effective stress of Bishop [34] where the stress term is defined as:

$$\sigma'_{ij} = \sigma_{ij} + \delta_{ij}(S_w p_w + S_a p_a) \tag{4}$$

In Eq. (4), σ_{ij} is the total stress tensor, δ is the Kronecker symbol while p_w and p_a are the pore water pressure and the pore air pressure assuming immiscibility of the two fluids. As found by Biot and Willis [35] Eq. (4) above can be modified to account for the volumetric deformation of the soil particles in the following way

$$\sigma'_{ij} = \sigma_{ij} + \alpha\delta_{ij}(S_w p_w + S_a p_a) \tag{5}$$

where

$$\alpha = 1 - K_T/K_S \tag{6}$$

where K_T and K_S are bulk modules of the porous medium and of the solid phase, respectively. The correction induced by factor α is negligible in most soils where usually K_S is much bigger than K_T but can assume relevance when rocks are concerned.

If only small deformations are considered, the stress-strain relationship for the porous medium can be written in an incremental form:

$$d\sigma'_{ij} = D_{T,ijkl}(d\varepsilon_{kl} - d\varepsilon^0_{kl}) \tag{7}$$

where $D_{T,ijkl}$ is the fourth order tangential stiffness tensor of the material, $d\varepsilon_{kl}$ the second order tensor describing the total strain increment and $d\varepsilon^0_{kl}$ is the fraction of the strain increment not induced by the effective stress.

3. Governing equations, finite element discretization and boundary conditions

The motion of the total mixture is defined by the motion of the solid-fluid mixture and the relative motion of the fluid with respect to the mixture. In this multiphase material model description it is common to present the motion of fluids relative to the motion of the solid phase in which the velocity is described by Darcy law [14]. Thus, the fluids relative velocities for water and air phases ($\dot{\boldsymbol{u}}^{ws}$ and $\dot{\boldsymbol{u}}^{as}$) are given by

$$\begin{aligned}\dot{\boldsymbol{u}}^{ws}(x,t) &= \dot{\boldsymbol{u}}^{w}(x,t) - \dot{\boldsymbol{u}}^{s}(x,t)\\ \dot{\boldsymbol{u}}^{as}(x,t) &= \dot{\boldsymbol{u}}^{a}(x,t) - \dot{\boldsymbol{u}}^{s}(x,t)\end{aligned} \tag{8}$$

In the above Eq. (8) $\dot{\boldsymbol{u}}^{ws}$ stands for relative velocity of water phase with respect to solid phase, $\dot{\boldsymbol{u}}^{w}$ stands for velocity of water phase, $\dot{\boldsymbol{u}}^{s}$ stands for velocity of solid phase, $\dot{\boldsymbol{u}}^{as}$ represents the relative velocity of air phase with respect to solid phase and $\dot{\boldsymbol{u}}^{a}$ represents the velocity of air phase. Under the assumption of small strain theory and isothermal equilibrium, the linear momentum balance equation for the whole mixture, considering the inertial and viscosity forces, for a unit control volume can be written as [24]:

$$\sigma_{kl,k} + \rho b = \rho\ddot{u} + \varsigma\dot{u} + nS_w\rho_w[\ddot{u}^{ws} + \mathrm{grad}\dot{u}^{w}\dot{u}^{ws}] + nS_a\rho_a[\ddot{u}^{wa} + \mathrm{grad}\dot{u}^{a}\dot{u}^{as}] \tag{9}$$

where b is the body force, ς is the damping parameter which is given a small value in order to minimize the damping effects in the computations and ρ is the averaged density of the mixture which can be written as:

$$\rho = (1-n)\rho_s + nS_w\rho_w + nS_a\rho_a \tag{10}$$

In Eq. (10), n is the porosity, ρ_s, ρ_w and ρ_a are the densities of solid, water and air phases respectively. Considering the low frequency domains as given in [18] Eq. (9) can be written as:

$$\sigma_{kl,k} + \rho b = \rho\ddot{u} + \varsigma\dot{u} \tag{11}$$

The linear momentum balance equation for each fluid phase yields simply the Darcy's law

$$\dot{u}_i^{s\pi} = k_\pi(-p_{\pi,i} + \rho_\pi(b_i - \ddot{u}_i)) \tag{12}$$

where $\dot{u}$ is the velocity of the fluid phase relative to the moving solid, π is either water or air phase and k_π is the permeability relative to the πth phase which is assumed to be isotropic. The dissipative terms arising in a multiphase flow system at the interfaces are taken into account through the relative permeability $k_{r\pi}$.

$$k_\pi = \frac{k}{\mu_\pi}k_{r\pi} \tag{13}$$

In Eq. (13) the term k is the intrinsic permeability, μ_π is the dynamic viscosity and $k_{r\pi}$ is the relative permeability of the water/air phase which depends on the relative saturation S_π through suitable experimental relationships $k_{r\pi} = k_{r\pi}(S_\pi)$.

The mass balance equation for each π phase may be written as:

$$S_\pi \frac{\alpha - n}{K_S}\dot{p} + \alpha S_\pi \dot{\varepsilon}_{ii} + n\dot{S}_\pi + \dot{u}^{s\pi}_{i,i} + S_\pi \frac{n}{\rho_\pi}\dot{\rho}_\pi = 0 \tag{14}$$

The first two terms in (14) represent the rate of change of grain volume due to average pressure changes, effective stress changes and total strain rate; the third term is the rate of change of saturation; the fourth term represents the net outflow from the control volume and the last one is the fluid density rate. The term $\dot{p}$ is the pressure change with respect to time while S_π is the degree of saturation for the phase π.

Taking into account Eqs. (1), (2) and (5) the following expressions are obtained

$$\dot{p} = \frac{\partial p}{\partial t} = \left[S_w + (p_a + p_w)\frac{\partial S_w}{\partial p_c}\right]\frac{\partial p_w}{\partial t} + \left[S_a + (p_a + p_w)\frac{\partial S_w}{\partial p_c}\right]\frac{\partial p_a}{\partial t} \tag{15}$$

And

$$\frac{1}{\rho_\pi}\dot{\rho}_\pi = \frac{1}{K_\pi}\dot{p}_\pi \tag{16}$$

In order to derive the weak form of the governing equations Galerkin's method of weighted residuals is used to derive the weak form of the equilibrium equations. The trial functions $\mathbf{u}(\boldsymbol{x}, t)$ and $p_w(\boldsymbol{x}, t)$ are required to satisfy all essential boundary conditions and to be smooth enough to define the derivatives of equations. In addition, test functions $\delta\mathbf{u}(\boldsymbol{x}, t)$ and $\delta p_w(\boldsymbol{x}, t)$ are required to be smooth enough to vanish at the prescribed strong boundary conditions. As given in the work of the author [36] the discretized governing equation for the water phase can be written as follows:

$$\begin{aligned}&\left[S_w \frac{\alpha - n}{K_s}\left(S_w + \frac{\partial S_w}{\partial p_c}p_c\right) + \frac{n \cdot S_w}{K_w} - n\frac{\partial S_w}{K_w}\right]\dot{p}_w \\ &+ \left[S_w \frac{\alpha - n}{K_s}\left(1 - S_w - \frac{\partial S_w}{\partial p_c}p_c\right) + n\frac{\partial S_w}{p_c}\right]\dot{p}_a + \alpha S_w \dot{\varepsilon}^{ii} \\ &+ \nabla^T\left[\frac{\mathbf{k}k_{rw}}{\mu_w}(-grad(p_w) + \rho_w(\mathbf{g} - \ddot{\mathbf{u}}_s))\right] = 0\end{aligned} \tag{17}$$

where in particular, $\mathbf{k}$ is the intrinsic permeability tensor, k_{rw} the water relative permeability, μ_w the water viscosity, n is porosity. The governing equation for the air phase can be written as:

$$\begin{aligned}&\left[(1 - S_w)\frac{\alpha - n}{K_s}\left(S_w + \frac{\partial S_w}{\partial p_c}p_c\right) + \frac{n \cdot S_w}{K_w}\right]\dot{p}_w \\ &+ \left[(1 - S_w)\frac{\alpha - n}{K_s}\left(1 - S_w - \frac{\partial S_w}{\partial p_c}p_c\right) - n\frac{\partial S_w}{p_c} + n\frac{(1 - S_w)}{K_a}\right]\dot{p}_a \\ &+ \alpha(1 - S_w)\dot{\varepsilon}^{ii} + \nabla^T\left[\frac{\mathbf{k}k_{ra}}{\mu_a}(-grad(p_a) + \rho_a(\mathbf{g} - \ddot{\mathbf{u}}_s))\right] = 0\end{aligned} \tag{18}$$

where k_{ra} is the air relative permeability, μ_a is the air viscosity. The inflow and outflow fluxes have been described by Darcy's law for both water and air flows. The finite element discretization in space is carried out and u, p_w and p_a are chosen as basic variables. These are expressed in terms of their nodal values by means of shape functions $\mathbf{N^u}$ and $\mathbf{N^p}$:

$$\mathbf{u} = \mathbf{N^u}\bar{\mathbf{u}}, \quad p^w = \mathbf{N^p}\bar{\mathbf{p}}^{\boldsymbol{w}} \quad \textbf{and } p^a = \mathbf{N^p}\bar{\mathbf{p}}^{\boldsymbol{a}} \tag{19}$$

By substituting the piecewise interpolation functions of Eq. (19) into the governing Eqs. (16)–(18), the semi discretized non linear system of differential equations is obtained as follows:

$$\begin{aligned}&\left[\int_\Omega \mathbf{N^{P,T}}\left[S_w\frac{\alpha - n}{K_s}\left(S_w + \frac{\partial S_w}{\partial p_c}p_c\right) + \frac{n \cdot S_w}{K_w} - n\frac{\partial S_w}{\partial p_c}\right]\mathbf{N^P}d\Omega\right]\dot{\bar{\mathbf{p}}}_\mathbf{w} \\ &+ \left[\int_\Omega \mathbf{N^{P,T}}\left[S_w\frac{\alpha - n}{K_s}\left(1 - S_w + \frac{\partial S_w}{\partial p_c}p_c\right) + \frac{n \cdot S_w}{K_w}\right]\mathbf{N^P}d\Omega\right]\dot{\bar{\mathbf{p}}}_\mathbf{a} \\ &+ \left[\int_\Omega \mathbf{N^{P,T}}\frac{kk_{rw}}{\mu_w}grad(\mathbf{N^P})d\Omega\right]\bar{\mathbf{p}}_\mathbf{w} + \left[\int_\Omega \nabla\mathbf{N^{P,T}}\frac{kk_{rw}}{\mu_w}\rho_w(\mathbf{N^U})d\Omega\right]\ddot{\mathbf{u}}_\mathbf{w} \\ &+ \left[\int_\Omega \mathbf{N^{P,T}}\alpha S_w\mathbf{m^T}\mathbf{B}d\Omega\right]\dot{\bar{\mathbf{u}}} + = \left[\int_\Omega \nabla\mathbf{N^{P,T}}\frac{kk_{rw}}{\mu_w}\rho_w(\mathbf{g})d\Omega\right] \\ &- \left[\int_{\Gamma w} \nabla\mathbf{N^{P,T}}\rho_w\frac{kk_{rw}}{\mu_w}(-\nabla(\mathbf{N^P}\bar{\mathbf{p}}_\mathbf{w}) + \rho_w(\mathbf{g}))^T\mathbf{n}d\Gamma\right]\end{aligned} \tag{20}$$

Eq. (20) is obtained for the water phase. Following the same procedure, the equation for the air phase can be written as:

$$\begin{aligned}&\left[\int_\Omega \mathbf{N^{P,T}}\left[(1 - S_w)\frac{\alpha - n}{K_s}\left((1 - S_w) - \frac{\partial S_w}{\partial p_c}p_c\right) + \frac{n \cdot (1 - S_w)}{K_w} - n\frac{\partial S_w}{\partial p_c}\right]\mathbf{N^P}d\Omega\right]\dot{\bar{\mathbf{p}}}_\mathbf{a} \\ &+ \left[\int_\Omega \mathbf{N^{P,T}}\left[(1 - S_w)\frac{\alpha - n}{K_s}\left(S_w + \frac{\partial S_w}{\partial p_c}p_c\right) + \frac{n \cdot \partial S_w}{\partial p_c}\right]\mathbf{N^P}d\Omega\right]\dot{\bar{\mathbf{p}}}_\mathbf{w} \\ &+ \left[\int_\Omega \nabla\mathbf{N^{P,T}}\frac{kk_{ra}}{\mu_a}grad(\mathbf{N^P})d\Omega\right]\bar{\mathbf{p}}_\mathbf{a} + \left[\int_\Omega \nabla\mathbf{N^{P,T}}\frac{kk_{ra}}{\mu_a}\rho_a(\mathbf{N^U})d\Omega\right]\dot{\bar{\mathbf{u}}} \\ &+ \left[\int_\Omega \mathbf{N^{P,T}}\alpha(1 - S_w)\mathbf{m^T}\mathbf{B}d\Omega\right]\dot{\bar{\mathbf{u}}} + = \left[\int_\Omega \nabla\mathbf{N^{P,T}}\frac{kk_{rw}}{\mu_w}\rho_w(\mathbf{g})d\Omega\right] \\ &- \left[\int_{\Gamma w} \nabla\mathbf{N^{P,T}}\rho_a\frac{kk_{ra}}{\mu_a}(-\nabla(\mathbf{N^P}\bar{\mathbf{p}}_\mathbf{a}) + \rho_a(\mathbf{g}))^T\mathbf{n}d\Gamma\right]\end{aligned} \tag{21}$$

The governing equation for the solid phase follows:

$$\begin{aligned}&\left[\int_\Omega \mathbf{B^T}\mathbf{D}_\mathbf{t}\mathbf{B}d\Omega\right]\bar{\mathbf{u}} - \left[\int_\Omega \mathbf{B^T}\mathbf{m^T}\alpha S_w\mathbf{N^P}d\Omega\right]\bar{\mathbf{p}}_\mathbf{w} \\ &- \left[\int_\Omega \mathbf{B^T}\mathbf{m^T}\alpha S_a\mathbf{N^P}d\Omega\right]\bar{\mathbf{p}}_\mathbf{a}\int_\Omega \mathbf{N^{U,T}}((1 - n)\rho_s + nS_w\rho_w + nS_a\rho_a)\mathbf{g}d\Omega \\ &- \left[\int_\Omega \mathbf{N^{U,T}}((1 - n)\rho_s + nS_w\rho_w + nS_a\rho_a)\mathbf{N^U}d\Omega\right]\ddot{\bar{\mathbf{u}}} \\ &- \left[\int_\Omega \mathbf{N^{U,T}}\varsigma\mathbf{N^U}d\Omega\right]\dot{\bar{\mathbf{u}}} + \int_\Gamma \mathbf{N^{U,T}}\mathbf{I^U}\sigma d\Gamma = 0\end{aligned} \tag{22}$$

In Eqs. (20)–(22) the matrix $\mathbf{B}$ refers to the strain operator and is given as follows:

$$\mathbf{B} = \begin{bmatrix}\frac{\partial N^u}{\partial x} & 0 \\ 0 & \frac{\partial N^u}{\partial y} \\ \frac{\partial N^u}{\partial y} & \frac{\partial N^u}{\partial x}\end{bmatrix} \tag{23}$$

and

$$\boldsymbol{\sigma}' = \mathbf{D_t}\boldsymbol{\varepsilon} = \mathbf{D_t}\mathbf{L}\mathbf{N^U}\bar{\mathbf{u}} = \mathbf{D_t}\mathbf{B}\bar{\mathbf{u}} \tag{24}$$

Eqs. (20)–(23) can be written in a matrix form as follows:

$$\begin{aligned}&\begin{bmatrix}\mathbf{M} & \mathbf{0} & \mathbf{0} \\ \mathbf{M_w} & \mathbf{0} & \mathbf{0} \\ \mathbf{M_a} & \mathbf{0} & \mathbf{0}\end{bmatrix}\begin{bmatrix}\dot{\bar{\mathbf{u}}} \\ \mathbf{0} \\ \mathbf{0}\end{bmatrix} + \begin{bmatrix}\mathbf{C} & \mathbf{0} & \mathbf{0} \\ \mathbf{C_{sw}^T} & \mathbf{P_{ww}} & \mathbf{C_{wa}} \\ \mathbf{C_{sa}^T} & \mathbf{C_{aw}} & \mathbf{P_{aa}}\end{bmatrix}\begin{bmatrix}\dot{\bar{\mathbf{u}}} \\ \dot{\bar{\mathbf{p}}}_\mathbf{w} \\ \dot{\bar{\mathbf{p}}}_\mathbf{a}\end{bmatrix} + \begin{bmatrix}\mathbf{0} & -\mathbf{C_{ws}^T} & \mathbf{C_{as}^T} \\ \mathbf{0} & \mathbf{H_{ww}} & \mathbf{0} \\ \mathbf{0} & \mathbf{0} & \mathbf{H_{aa}}\end{bmatrix}\begin{bmatrix}\bar{\mathbf{u}} \\ \bar{\mathbf{p}}_\mathbf{w} \\ \bar{\mathbf{p}}_\mathbf{a}\end{bmatrix} \\ &+ \int_\Omega \mathbf{B^T}\sigma\prime d\Omega = \begin{bmatrix}\mathbf{f_u} \\ \mathbf{f_w} \\ \mathbf{f_a}\end{bmatrix}\end{aligned} \tag{25}$$

The developed multiphase model is implemented in the finite element software ANSYS [37] by using the programmable features of the software. More detailed explanation for the implementation of the multiphase model into the finite element software ANSYS can be found in the work of the author [36]. In Eq. (25) the mass matrices for solid, water and air phases ($\mathbf{M}$, $\mathbf{M}_w$ and $\mathbf{M}_a$) can be given as follows:

$$\mathbf{M} = \int \mathbf{N}_u[\rho_s(1 - n) + nS_w\rho_w]\mathbf{N}_u d\Omega \tag{26}$$

$$\mathbf{M}_w = \int \nabla\mathbf{N}_p^T\frac{\mathbf{k}k_{rw}}{\eta_w}\rho_w\mathbf{N}_u d\Omega \tag{27}$$

$$\mathbf{M}_a = \int \nabla \mathbf{N}_p^T \frac{\mathbf{k} k_{ra}}{\eta_a} \rho_a \mathbf{N}_u d\Omega \tag{28}$$

The coupling matrices among solid (s), water (w) and air (a) are given as:

$$C_{ws} = \int \mathbf{N}_p^T \alpha S_w \mathbf{m}^T \mathbf{L} \mathbf{N}_u d\Omega \tag{29}$$

$$C_{ws} = \int \mathbf{N}_p^T \alpha S_w \mathbf{m}^T \mathbf{L} \mathbf{N}_u d\Omega \tag{30}$$

$$C_{wa} = \int \mathbf{N}_p^T \left[(\alpha - n) \left(S_a - p_c \frac{\partial S_w}{\partial p_c} \right) - n \frac{\partial S_w}{\partial p_c} \right] \mathbf{N}_p d\Omega \tag{31}$$

$$C_{aw} = \int \mathbf{N}_p^T \left[\frac{S_w}{K_s} (\alpha - n) \left(S_w + p_c \frac{\partial S_w}{\partial p_c} \right) - n \frac{\partial S_w}{\partial p_c} \right] \mathbf{N}_p d\Omega \tag{32}$$

The compressibility matrices of water and air phases can be written as:

$$P_{ww} = \int \mathbf{N}_p^T \left[\frac{S_w}{K_w} + (\alpha - n) \frac{S_w}{K_s} \left(S_w + p_c \frac{\partial S_w}{\partial p_c} \right) - n \frac{\partial S_w}{\partial p_c} \right] \mathbf{N}_p d\Omega \tag{33}$$

$$P_{aa} = \int \mathbf{N}_p^T \left[\frac{n S_a}{K_a} + (\alpha - n) \frac{S_a}{K_s} \left(S_a + p_c \frac{\partial S_w}{\partial p_c} \right) - n \frac{\partial S_w}{\partial p_c} \right] \mathbf{N}_p d\Omega \tag{34}$$

The permeability matrices of water (H_{ww}) and air (H_{aa}) phases are given as:

$$H_{ww} = \int \nabla \mathbf{N}_p^T \frac{\mathbf{k} k_{rw}}{\eta_w} \nabla \mathbf{N}_p d\Omega \tag{34}$$

$$H_{aa} = \int \nabla \mathbf{N}_p^T \frac{\mathbf{k} k_{ra}}{\eta_a} \nabla \mathbf{N}_p d\Omega \tag{35}$$

The domain forces for solid, water and air phases are given as:

$$f_u^{\Omega} = \int \mathbf{N}_u [\rho_s (1 - n) + n S_w \rho_w + n S_a \rho_a] \mathbf{g} \mathbf{N}_u d\Omega \tag{36}$$

$$f_{pw}^{\Omega} = \int \mathbf{N}_p^T \frac{\mathbf{k} k_{rw}}{\eta_w} \rho_w \mathbf{g} d\Omega \tag{37}$$

$$f_{pa}^{\Omega} = \int \mathbf{N}_p^T \frac{\mathbf{k} k_{ra}}{\eta_a} \rho_a \mathbf{g} d\Omega \tag{38}$$

The term $\int \mathbf{B}^T \sigma' d\Omega$ incorporates the material model of the solid phase which can be either linear or nonlinear in which $\mathbf{B}^T$ stands for the displacement-strain transformation matrix, σ' is the vector form of the effective stress tensor at the integration points and Ω is the domain concerned.

At each node of the element, four degrees of freedom are defined. Since the model is in plane strain, the displacement is considered in two directions. Pore water and pore air pressures are added also on the nodes thus making four degrees of freedom at each node. The system is non symmetric and coupled meaning that it cannot solve any field separately from others. In Eq. (25) u, p_w and p_a denote the global vectors of the nodal values for the displacements of the soil skeleton and for the hydrostatic stresses in the fluid phases of water and air. The coupling matrices C_{sw}, C_{sa} and C_{wa} reflect the coupling between the individual constituents. The compressibility matrices P_{ww} and P_{aa} contain the compressibility of the particular fluid and the derivative of the degree of water saturation with respect to the capillary stress. The permeability matrices H_{ww} and H_{aa} depend on the permeabilities of the soil skeleton with respect to both fluid phases of water and air.

Due to the nonlinearity of the coupled problem, an iterative procedure must be used to solve the system of equations. A Newton Raphson scheme is adopted to linearise the problem.

The introduced governing equations from the boundary value problem can be solved using the appropriate initial and boundary conditions. The solid phase boundary conditions are $\mathbf{u} = \bar{\mathbf{u}}$ on $\Gamma = \Gamma_u$ and $\mathbf{t} = \boldsymbol{\sigma}\mathbf{n} \equiv \bar{\mathbf{t}}$ on $\Gamma = \Gamma_t$ where the whole boundary is a union of traction and displacement boundaries such as $\Gamma = \Gamma_u + \Gamma_t$. The fluid phase boundary conditions are $\mathbf{p} = \bar{\mathbf{p}}$ on $\Gamma = \Gamma_p$ and $\mathbf{n}\mathbf{w} = \mathbf{n} \cdot \mathbf{k}(-\nabla p_w + S_w \rho_f \mathbf{b})$ on $\Gamma = \Gamma_w$ with $\Gamma = \Gamma_p + \Gamma_w$.

4. Constitutive relations

In this section, a constitutive model is presented for soil skeleton that is capable of predicting the material behavior accurately. The behavior of the solid skeleton is assumed to be described as both linear and nonlinear. In the case of a linear material, the stress-strain relation is defined as follows:

$$\sigma_{ij} = E_{ijkl} \varepsilon_{kl} \tag{39}$$

The linear elastic material model is used for very tiny space of soil modeling where deformations are in small ranges where the coupling of water and air phases are of primary interest. In the case of nonlinear simulation, the hypoplastic material model is used. The hypoplastic constitutive laws [38–40] are an alternative to the elasto-plastic formulations for continuum modeling of granular materials. They describe the evolution of effective stress components with the evolution of strain components by a differential equation including isotropic linear and non-linear tensorial functions. The hypoplastic constitutive laws are of the rate type. Due to the incremental non-linearity with the deformation rate, they are able to describe both a non-linear stress–strain and volumetric behavior of granular bodies during shearing up to and after the peak with a single tensorial equation. For completeness, the formulas are presented further in the text.

The hypoplastic constitutive equation by von Wolffersdorff [38] is given in Eq. (40).

$$\Delta \sigma'_{ij} = L_{ijkl} \Delta \varepsilon_{kl} + N_{ij} \sqrt{\Delta \varepsilon_{kl} \Delta \varepsilon_{kl}} \tag{40}$$

The term L_{ijkl} is a fourth order tensor describing the linear relation between the strain and stress rates and N_{ij} represents the nonlinear part.

$$L_{ijkl} = f_s \frac{1}{\hat{\sigma}_{mn} \cdot \hat{\sigma}_{mn}} (F^2 I_{ijkl} + a^2 \hat{\sigma}_{ij} \cdot \hat{\sigma}_{ij}) \tag{41}$$

$$N_{ij} = f_s f_d \frac{Fa}{\hat{\sigma}_{kl} \cdot \hat{\sigma}_{kl}} (\hat{\sigma}_{ij} + \hat{\sigma}^*_{ij}) \tag{42}$$

The term I_{ijkl} is the fourth order unity tensor given by

$$I_{ijkl} = 0.5(\delta_{ik}\delta_{jl} + \delta_{il}\delta_{jk}) \tag{43}$$

The normalized Cauchy stress tensor and its deviatoric parts are defined by:

$$\hat{\sigma}_{ij} = \frac{\sigma'_{ij}}{tr(\sigma)} \tag{44}$$

$$\hat{\sigma}^*_{ij} = \hat{\sigma}_{ij} - \frac{1}{3} I \tag{45}$$

Factor a depends on the critical friction angle phi and is defined as:

$$a = \frac{\sqrt{3}(3 - sin\varphi_c)}{2\sqrt{2} sin\varphi_c} \tag{46}$$

The scalar factors $fs = fs(e,\sigma_{kk})$ and $fd = fd(e,\sigma_{kk})$ take into account the influence of the density and pressure level on stress. The stiffness factor f_s given in Eq. (47) is proportional to the granulate hardness h_s and depends on the mean stress and void ratio. The granulate hardness h_s represents a density-independent reference pressure and it is related to the entire skeleton (not to single grains). The density factor f_d resembles a pressure-dependent relative density index and is represented by Eq. (48).

$$f_s = \frac{h_s}{n}\left(\frac{e_i}{e}\right)^{\beta} \times \frac{1+e_i}{e_i}\left(-\frac{\sigma_{ij}\delta_{ij}}{h_s}\right)^{1-n} x\left[3+a^2-\sqrt{3}\left(\frac{e_{i0}-e_{d0}}{e_{c0}-e_{d0}}\right)^{\alpha}\right]^{-1} \quad (47)$$

$$f_d = \left(\frac{e-e_d}{e_c-e_d}\right)^{\alpha} \quad (48)$$

In the Eqs. (47) and (48) the parameters α and β indicate the exponents which relate the dependence of the peak friction angle on granulometric properties. A detailed description is given in the work of Herle and Gudehus [40]. The actual void ratios e_x are obtained with the initial void ratios e_{x0}, the stress state σ and the parameters h_s and n from the following equation:

$$\frac{e_i}{e_{i0}} = \frac{e_c}{e_{c0}} = \frac{e_d}{e_{d0}} = \frac{e}{e_0} = exp\left[-\left(-\frac{\sigma'_{ij}\delta_{ij}}{h_s}\right)^{n}\right] \quad (49)$$

The hypoplastic material model describes the relation between minimum void ratio e_d which decreases with pressure p_s according to the following relation

$$e_{d0} = e_d \exp\left[\left(\frac{3p_s}{h_s}\right)^{n}\right] \quad (50)$$

As stated in the work of Herle and Gudehus [40] for determination of h_s and n used in Eqs. (49) and (50), a compression test with an initially very loose (but not collapsible) specimen has to be performed. The performed tests at the Laboratory for Geodynamics at the Institute of Earthquake Engineering and Engineering Seismology in Skopje, Macedonia (IZIIS) revealed values of $h_s = 2620$ [MPa] and $n = 0.269$ which slightly differ from the values obtained by Herle and Gudehus [40]. Detailed description of the tests is given in the work of the first author [36]. The pressure dependent parameters e_i and e_d represent the maximum and minimum void ratios, while the parameter e_c corresponds to the critical void ratio. Consequently, the parameters e_{i0}, e_{d0} and e_{c0} correspond to the initial values of the maximum, minimum and critical void ratios.

The function F(σ) determined by fitting the yield condition by Matsuoka-Nakai is included as follows:

$$F = \sqrt{\frac{1}{8}tan^2\psi + \frac{2-tan^2\psi}{2+\sqrt{2}tan\psi cos3\theta}} - \frac{1}{2\sqrt{2}}tan\psi \quad (51)$$

In Eq. (51) the terms θ and ψ are related as follows:

$$\cos 3\theta = -\sqrt{6}\frac{\hat{\sigma}^*_{ij}\hat{\sigma}^*_{jk}\hat{\sigma}^*_{ki}}{(\hat{\sigma}^*_{mn}\hat{\sigma}^*_{mn})^{\frac{3}{2}}} \quad (52)$$

$$\tan\psi = -\sqrt{3}\sqrt{\hat{\sigma}^*_{kl}\hat{\sigma}^*_{kl}} \quad (53)$$

The rate of void ratio is expressed by the following equation:

$$\dot{e} = (1+e)tr\mathbf{D} \quad (54)$$

Although vonWolffersdorff's hypoplastic constitutive equation reliably predicts the nonlinear inelastic behavior of soil, there are some drawbacks with respect to its application to cyclic stress conditions.

The most severe shortcoming is the excessive accumulation of deformations for small stress cycles, a phenomenon called ratcheting. To overcome these drawbacks, Niemunis and Herle [41] presented an extension of the hypoplastic constitutive equation by introducing the concept of intergranular strain. In addition to the deformations of the granular structure by grain rearrangement, they also take the deformations of the contact area between the distinct grains into account. The modified version of Eq. (40) is then transformed to the form of Eq. (55).

$$\Delta\sigma'_{ij} = M_{ijkl}\Delta\varepsilon_{kl} \quad (55)$$

with

$$M_{ijkl} = [\rho^k m_T + (1-\rho^k)m_R]L_{ijkl} + \rho^k(1-m_T)L_{ijmn}\widehat{S}_{mn}\widehat{S}_{kl} + \rho^k N_{ij}\widehat{S}_{kl} \quad (56)$$

$$M_{ijkl} = [\rho^k m_T + (1-\rho^k)m_R]L_{ijkl} + \rho^k(m_R-m_T)L_{ijmn}\widehat{S}_{mn}\widehat{S}_{kl} \quad (57)$$

Here S_{ij} is an additional variable representing the intergranular strain. Its rate of change is determined from the following equation.

$$\Delta S_{ij} = \begin{Bmatrix} (I_{ijkl} - \rho^{\beta}R\widehat{S}_{ij}\widehat{S}_{kl})\Delta\varepsilon_{kl} \\ \Delta\varepsilon_{kl} \end{Bmatrix} \quad (58)$$

For the fluids in the coupled model relationships between saturation, permeability and capillary pressure have been selected accordingly. The hysteretic behavior exhibited under cycles of wetting and drying is not considered in this study.

5. Numerical simulation and implementation in ANSYS software

In order to illustrate the accuracy of the newly developed coupled model several numerical examples including elastic soil column and simulation of experimental results are presented. The first two examples are chosen to assess the accuracy of the proposed coupled model for two quasi static problems of partially saturated media. Next, simulation of experimental results is presented by considering the soil as fully saturated while the behavior of the soil skeleton is simulated by the hypoplastic material model. The user subroutines in the ANSYS software are good tools that enable the user to define the proper material and or element needed to treat a given mathematical problem. In this paper, UEL101 was used to introduce the desired formulations within the framework of the numerical model. In this case, ANSYS calls the UEL subroutine at every element in the domain. ANSYS passes material properties, initial conditions and boundary conditions to UEL through the assigned interphase of the software. The stresses, stiffness matrix and internal state variables are updated and passed back to ANSYS by the UEL. The UEL consists of two parts A and B as shown in Fig. 1. After the convergence is obtained the values of part A are written to part B from which all state variables are stored in ANSYS to be used at the next time step.

As can be seen from Fig. 1 in order to integrate the material model at element level, the user element of ANSYS software is divided into two parts A and B. The iteration ends when there is convergence of the results in the element level. When iteration begins the loop of numerical integration is activated in which initial values of stress, strain, void ratio and saturation are introduced. At the end of this iteration material stiffness matrix is calculated and returned to the ANSYS software.

In this work, the new point in integration is obtained by controlling the amount strain increment in the substeps. At this point, the amount of strain increment is directly related to the density of the specimen through the void ratio "e" given in the initial values at the beginning of the iteration. The relations are given in four steps relating the percentage of density increase to the amount of strain increment which is multiplied by a factor of multiplication.

Please cite this article in press as: Edip K et al. Development of coupled numerical model for simulation of multiphase soil. Comput Geotech (2017), https://doi.org/10.1016/j.compgeo.2017.08.016

From Table 1 it can be obtained that if the increase in density percentage is more than 10% the amount of the strain increment in the substep is multiplied by a factor of 0.5. If the increase in density percentage is less than 10% the amount of strain increment in the substep is multiplied by a corresponding factor of 0.2, 0.1 or 0.05. In this way the strain increment calculation is calibrated in order to obtain the stress values. The more detailed explanation is given in the PhD work of the first author [36]. The state variables are updated at each time step using the explicit Euler forward integration scheme. The developed element is an eight node quadrilateral element with two degrees of freedom (DOF) for displacement at each node and per one DOF for air and one DOF for water pressure as shown in Fig. 2.

The water and air pressure shape functions are of a linear type while the shape functions for the solid displacements are quadratic in order to simulate the solid displacements. An implicit type of solving has been adopted. The numeration of the nodes has been adopted to best fit the user programmable features UPF of the ANSYS software.

5.1. Simulation of drainage of a soil column – Liakopoulos test

The physical experiment of Liakopoulos was conducted through the soil column of Del Monte sand instrumented to measure mois-

Table 1
Substeps of strain increment calculation.

Percentage of density increase $D_{R\_increase}$	Factor of multiplication
$D_{R\_increase}$ > 10%	0.5
2% > $D_{R\_increase}$ >10%	0.2
1% > $\mathbf{D_{R\_increase}}$ > 2%	0.1
$\mathbf{D_{R\_increase}}$ < 1%	0.05

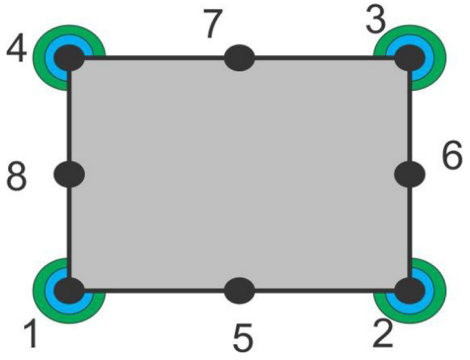

Fig. 2. Eight node quadrilateral element with two displacement DOF (black), one DOF for water pressure (blue) and one DOF for air pressure (green). (For interpretation of the references to colour in this figure legend, the reader is referred to the web version of this article.)

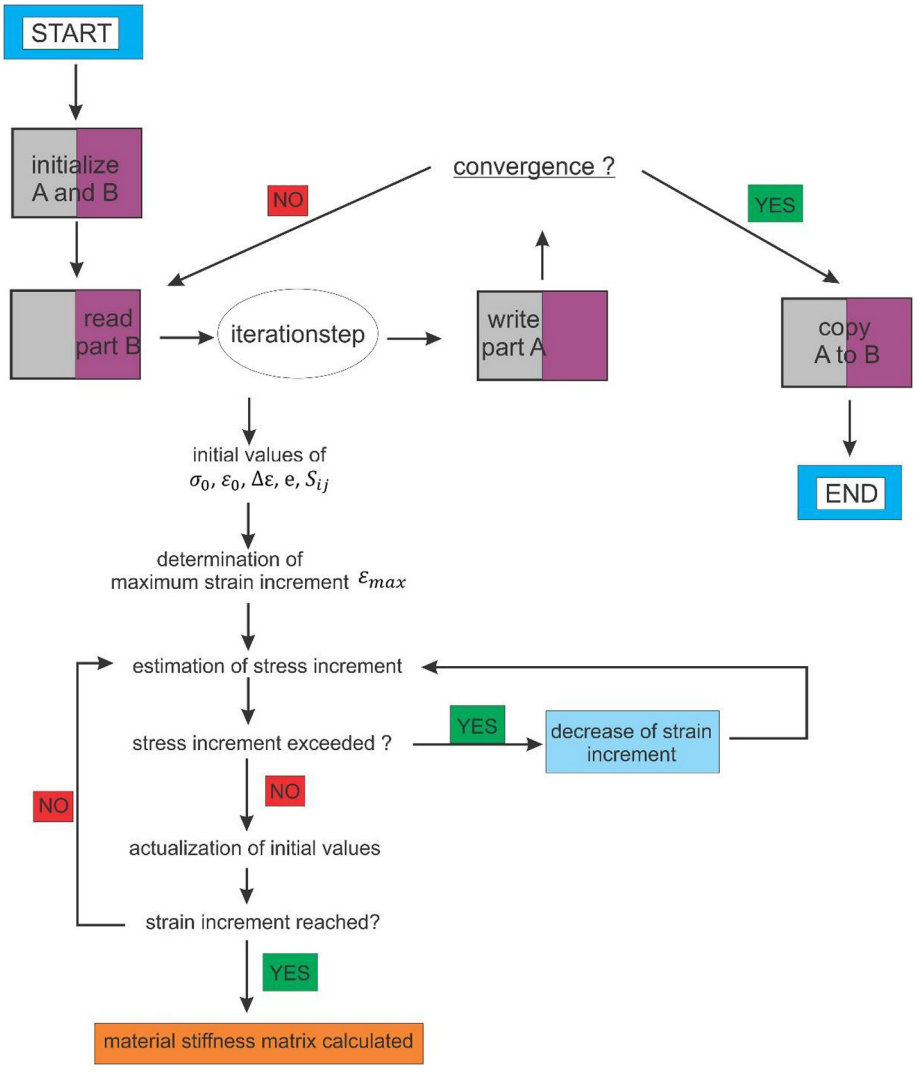

Fig. 1. Iteration and integration of hypoplastic material model at element level.

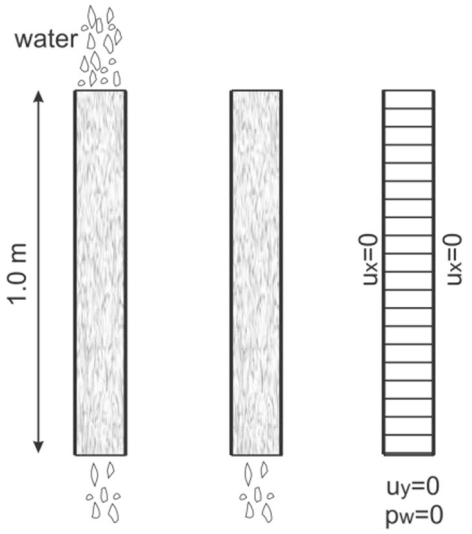

Fig. 3. Simulation of Liakopoulos drainage test.

ture tension at various points along height. Prior to the start of the experiment a constant flow through the column corresponding to a zero water pressure is imposed. At $t = 0$ sec, the water supply from the top surface is cut and water is left to flow out through the bottom of the soil column. The sand porosity and the dependence of water saturation and water permeability on water pressure were determined by Liakopoulos [28]. Since the problem is solved as both water and air flow problem, the relative air permeability is a function of capillary pressure. Numerical solutions can be found, e.g., in the book by Lewis and Schrefler [23] or other authors [24,29]. In particular, the benchmark is based on the assumption of a deformable linear elastic soil. The experiment conducted for the soil column has 1 m height and 0.1 m width and is shown in Fig. 3.

The mechanical parameters of the Del Monte Sand were taken based on the previous works of Schrefler and Scotta [24] and are given in the table below.

In order to simulate the seepage experiment of Liakopoulos the following relations are used:

$$S_w = 1 - 0.10152 \cdot (p_c/\rho_w g)^{2.4279}$$
$$k_{rw} = 1 - 2.207 \cdot (1 - S_w)^{1.0121}$$
$$k_{ra} = (1 - S_e)^2 (1 - S_e)^{(2+\lambda)/\lambda} \quad (59)$$

The simulated time domain, according to the experiments of Liakopoulos is set to two hours. In Figs. 4 and 5, the numerical results from the calculation by using coupled model and values from other authors for the water pressure, air pressure, displacement and saturation are shown. As can be seen from Figs. 4 and 5 the numerical model of this study predicts the results satisfactorily. Furthermore, it is evident that the maximal air suction at time t = 20 min significantly influences the water flow since the saturation percentage until then is above 90%. After 20 min the saturation is reduced to below 90% thus air flow into the soil column is allowed with smaller levels of suction pressure. The water pressure values in Fig. 5 show clearly that the flow of water is changed under the gravitational force with the increase in time. From the figures above it can be stated that the evolution of air pressure is more sensitive in comparison with the water pressure development. It is also to be noted that the transition between fully and partially saturated zones is positioned to nearly 0.2 m from the top of the column which is slightly different from the Liakopoulos simulation of Gawin et al. [22]. This is due to the fact that, in the work of Gawin et al. [22] only the static gas conditions are presented. On the other hand, the values obtained in this study are in complete agreement with the results given in the works of Schrefler and Scotta [24], Laloui et al. [42] and Khoei and Haghighat [43] where the simulation of both air and water pressures are considered with respect to time. It is to be mentioned that, since experimental air pressure and saturation were not recorded in the experiment performed by Liakopoulos comparisons are possible only with numerical results from other authors. Differences are mainly the result of choosing different sets of governing equations.

5.2. Consolidation of partially saturated column

In order to verify the proposed coupled method, in this example a partially saturated consolidation of a one meter long vertical soil column is simulated. This example aims to verify the proposed numerical model by comparing the simulation results with those of the Khoei and Mohammadnejad [29]. At the beginning the vertical soil column of 1 m height and 0.1 m width is subjected to a surface load of 1 kPa as shown in Fig. 6.

The vertical soil column is assumed to be partially saturated with an initial water saturation of 52% and the initial pore water pressure is set to be −280 kPa. Subsequently, the pore water pressure at the top surface is changed immediately from −280 kPa to −420 kPa while it is exposed to air pressure. The boundary condi-

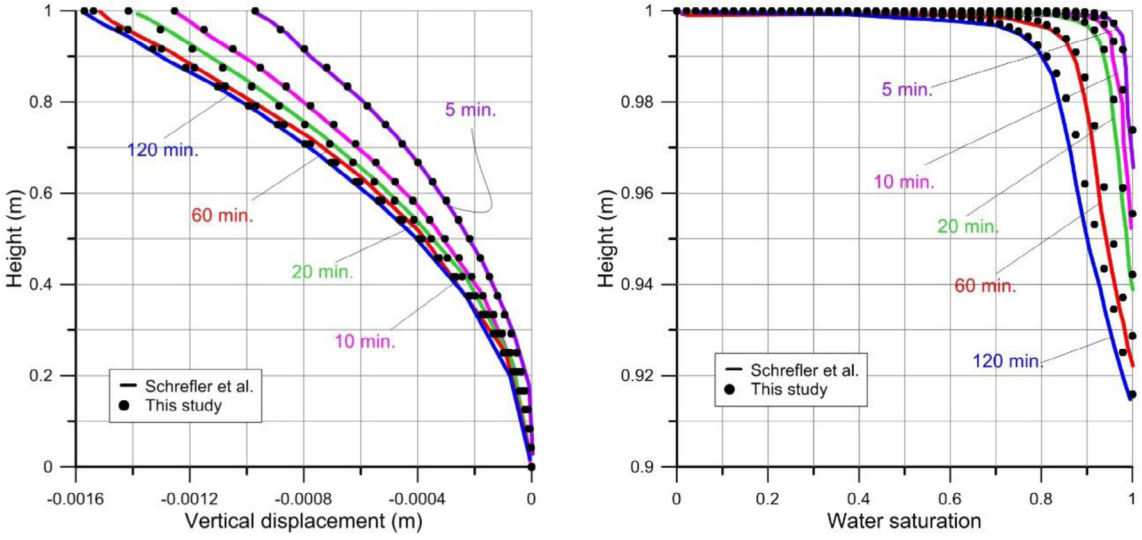

Fig. 4. Comparison of vertical displacement and water saturation through the height of a sand column.

Please cite this article in press as: Edip K et al. Development of coupled numerical model for simulation of multiphase soil. Comput Geotech (2017), https://doi.org/10.1016/j.compgeo.2017.08.016

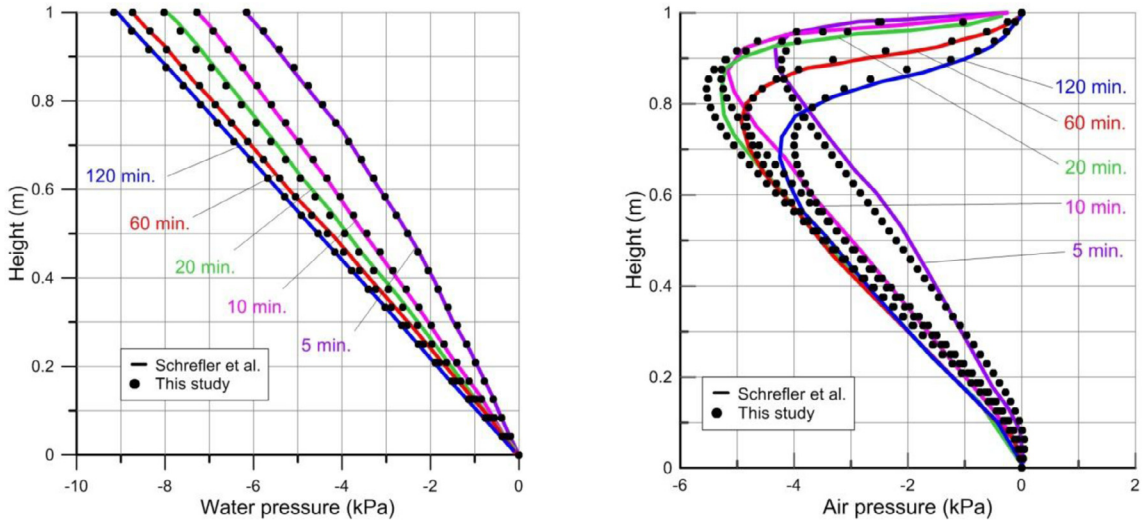

Fig. 5. Comparison of water and air pressure through the height of a sand column.

tions of the soil column are impermeable to water and air except the top surface which has drained boundaries. The vertical displacements are restrained at the bottom while both sides of the soil column have constrained horizontal displacements. The material parameters of the porous medium are given in Table 2.

In numerical simulation the water saturation-capillary pressure and the relative permeabilities of water and air phases are taken into consideration as given in Brooks and Corey [44] (see Tables 3 and 4).

$$S_w = S_{rw} + (1 - S_{rw})\left(\frac{p_b}{p_c}\right)^{\lambda} \tag{60}$$

The functions of the relative permeability of the water and air phase are:

$$k_{rw} = S_e^{(2+3\lambda)/\lambda} \tag{61}$$

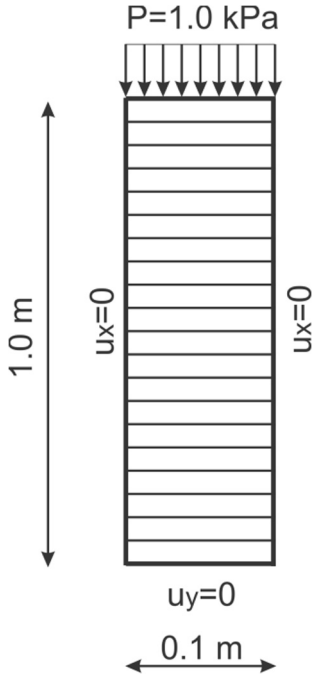

Fig. 6. Domain of partially saturated column.

Table 2
Parameters of del monte sand.

Description	Value
Young's modulus of elasticity	E = 1.3 MPa
Poisson's ratio	ν = 0.4
Solid grain density	ρ_s = 2000 kg/m^3
Bulk modulus of solid grains	$K_s = 1.0 \times 10^6$ MPa
Bulk modulus of water	$K_w = 2.0 \times 10^3$ MPa
Bulk modulus of air	K_a = 0.1 MPa
Water density	ρ_w = 1000 kg/m^3
Air density	ρ_a = 1.20 kg/m^3
Initial porosity	n = 0.2975
Intrinsic permeability	$k = 4.5 \times 10^{-13}$ m^2
Water viscosity	$\mu_w = 1.0 \times 10^{-3}$ Pa s
Air viscosity	$\mu_a = 1.8 \times 10^{-5}$ Pa s
Gravitational acceleration	g = 9.806 m s^{-2}
Atmospheric reference pressure	p_{atm} = 0.0 MPa

Table 3
Material parameters of the soil column.

Description	Value
Young's modulus of elasticity	E = 6 MPa
Poisson's ratio	ν = 0.4
Solid grain density	ρ_s = 2000 kg/m^3
Bulk modulus of solid grains	$K_s = 0.14 \times 10^{10}$ Pa
Bulk modulus of water	$K_w = 0.43 \times 10^{13}$ Pa
Bulk modulus of air	$K_a = 0.1 \times 10^6$ Pa
Water density	ρ_w = 1000 kg/m^3
Air density	ρ_a = 1.22 kg/m^3
Initial porosity	n = 0.3
Intrinsic permeability	$k = 0.46 \times 10^{-11}$ m^2
Water viscosity	$\mu_w = 1.0 \times 10^{-3}$ Pa s
Air viscosity	$\mu_a = 1.8 \times 10^{-3}$ Pa s
Gravitational acceleration	g = 9.806 m s^{-2}
Atmospheric reference pressure	p_{atm} = 101.0 kPa

Table 4
Hypoplastic parameters of Toyoura sand.

Description	Value
Angle of internal friction φ_c [°]	30
Granulate hardness h_s [MPa]	2650
Exponent n	0.26
Minimum void ratio e_{d0}	0.61
Critical void ratio e_{c0}	0.98
Maximum void ratio e_{i0}	1.09
Numerical parameter α	0.2
Numerical parameter β	1.0

Please cite this article in press as: Edip K et al. Development of coupled numerical model for simulation of multiphase soil. Comput Geotech (2017), https://doi.org/10.1016/j.compgeo.2017.08.016

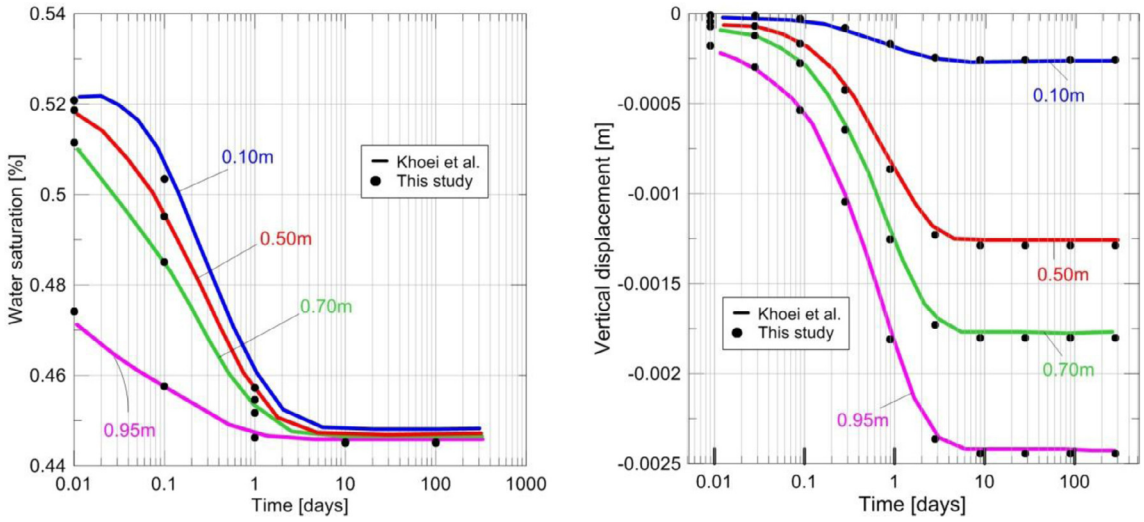

Fig. 7. Comparison of water saturation and vertical displacement versus time.

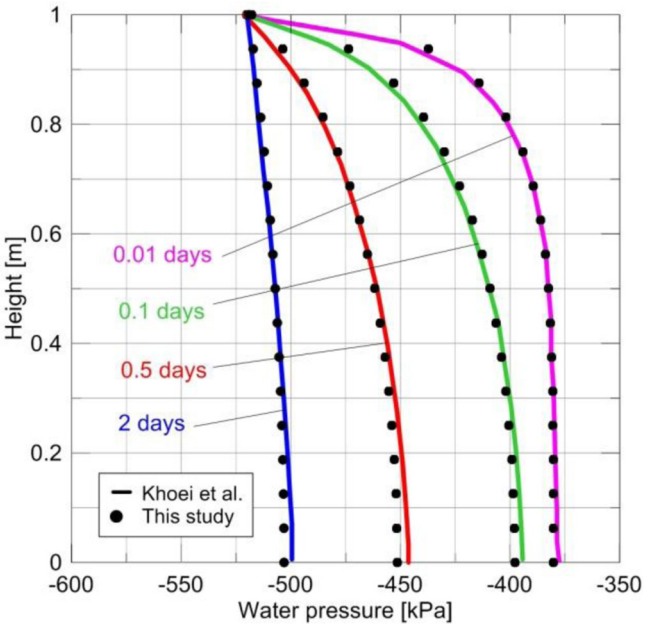

Fig. 8. Comparison of water pressure with respect to height of the column.

$$k_{rg} = (1 - S_e)^2 \left(1 - S_e^{(2+\lambda)/\lambda}\right) \tag{62}$$

The residual water saturation is set to $S_{rw} = 0.3966$ and the bubbling pressure $p_b = 225$ kN/m^2. The pore size distribution index λ is taken as 3 as in the work of Khoei and Mohammadnejad [29]. The comparison of water saturation and vertical displacement values with respect to time are plotted for the selected nodal points within the soil column.

As can be seen from Fig. 7 the computed distribution of water saturation and vertical displacement along the soil column match quit good with the numerical results of Khoei and Mohammadnejad [29]. Fig. 8 shows the comparison of computed distribution of water pressure using the proposed coupled method with respect to the numerical simulations presented by Khoei and Mohammadnejad [29].

From the results it is clearly seen that the coupling between water and air phases is simulated correctly in the developed coupled numerical model.

Fig. 9. Soil specimen on a triaxial apparatus.

Table 5
Hypoplastic parameters of Toyoura sand.

Description	Value
Angle of internal friction φ_c [°]	30
Granulate hardness h_s [MPa]	2620
Exponent n	0.269
Minimum void ratio e_{d0}	0.61
Critical void ratio e_{c0}	0.98
Maximum void ratio e_{i0}	1.09
Numerical parameter α	0.2
Numerical parameter β	1.0
Hypo r	0.0001
Hypo m_R	5.0
Hypo m_T	2.0
Hypo β_R	0.25
Hypo γ	6.0

5.3. Simulation of triaxial experiments

5.3.1. Simulation of static – monotonic triaxial experiments

The coupled model is used to simulate monotonic triaxial experiments performed at the Laboratory for Geodynamics at the Institute of Earthquake Engineering and Engineering Seismology in Skopje, Macedonia (IZIIS). The measuring soil sample is proportioned 70 × 140 mm, as shown in Fig. 9.

Please cite this article in press as: Edip K et al. Development of coupled numerical model for simulation of multiphase soil. Comput Geotech (2017), https://doi.org/10.1016/j.compgeo.2017.08.016

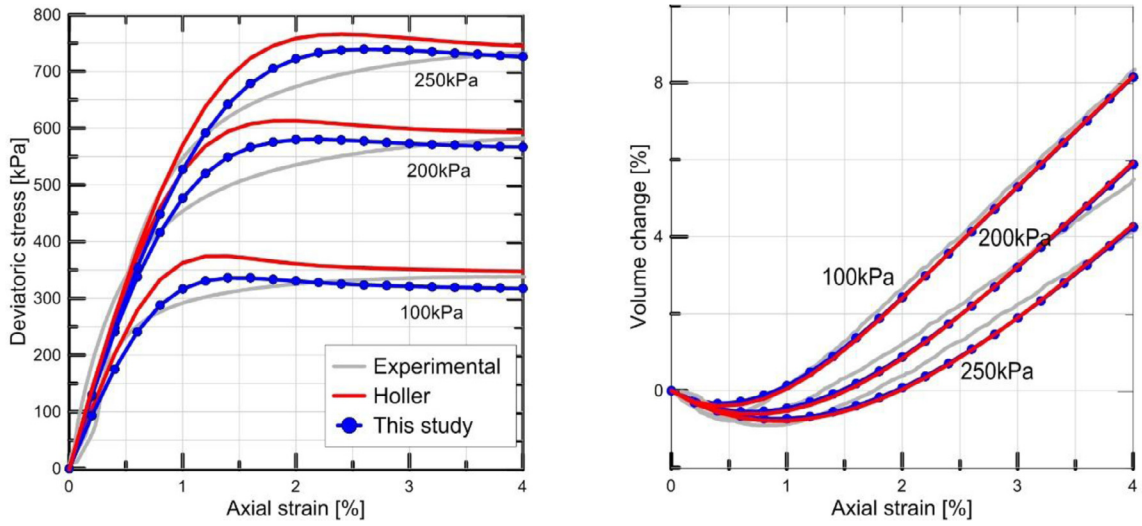

Fig. 10. Comparison between numerical and experimental values in drained conditions.

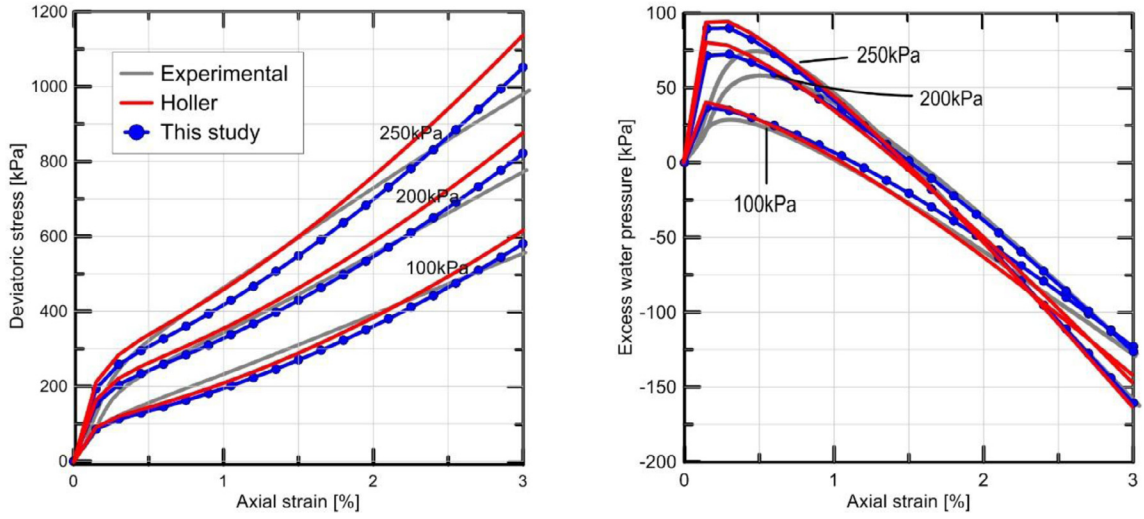

Fig. 11. Comparison between numerical and experimental values in undrained conditions.

The plots of stress versus axial strain and volumetric versus axial strain relationships of Toyoura sand are simulated by the coupled model. The constitutive equation for the solid state in the multiphase model is the hypoplastic material model as given in Eq. (40). The numerical model is found to respond to the changes in confining pressure and the initial relative density of a given granular material. The results are obtained for three confining pressures (100, 200 and 250 kPa) at approximately the same initial void ratio of $D_R = 0.75$. In order to implement the hypoplastic material model in the numerical analysis, the parameters for the Toyoura sand were defined at the Laboratory for Geodynamics at the Institute of Earthquake Engineering and Engineering Seismology in Skopje, Macedonia (IZIIS-Skopje). The procedures used for defining the parameters followed the description of Herle [45]. The obtained parameters for Toyoura sand at IZIIS-Skopje can be summarized as in Table 5. The values for granulate hardness h_s and exponent n are slightly different from the values obtained of Herle [46]. This is due to the type of the Toyoura sand which has been used in experiments at the Laboratory for Geodynamics at the Institute of Earthquake Engineering and Engineering Seismology.

In simulating the monotonic compression tests, both drained and undrained conditions are considered. In drained tests, pore pressure development is disabled due to the open valve in the water flow. The main measuring part in the experiment is the volume change measuring the amount of water flow outside of the soil sample. Fig. 10 shows comparison of the experimental with the numerical results of the coupled method. The newly developed multiphase model seems to give better results when compared with the reference model of Holler [27]. This is mainly due to the integration of the constitutive model which improves the stress values at the end of the iterations.

In the undrained tests, pore pressure development is considered as the valve is closed hindering the water flow. The main measuring part in the experiment is the deviatoric stress and the pore water pressure. In Fig. 11 comparison between experimental and numerical results is presented.

Regarding the results, it should be mentioned that Figs. 10 and 11 clearly demonstrate the influence of confining pressure on stress development in the samples. As can be seen from the figures above, there is a good relation between the numerical and the experimental results. Increasing the confining pressure has led

Please cite this article in press as: Edip K et al. Development of coupled numerical model for simulation of multiphase soil. Comput Geotech (2017), https://doi.org/10.1016/j.compgeo.2017.08.016

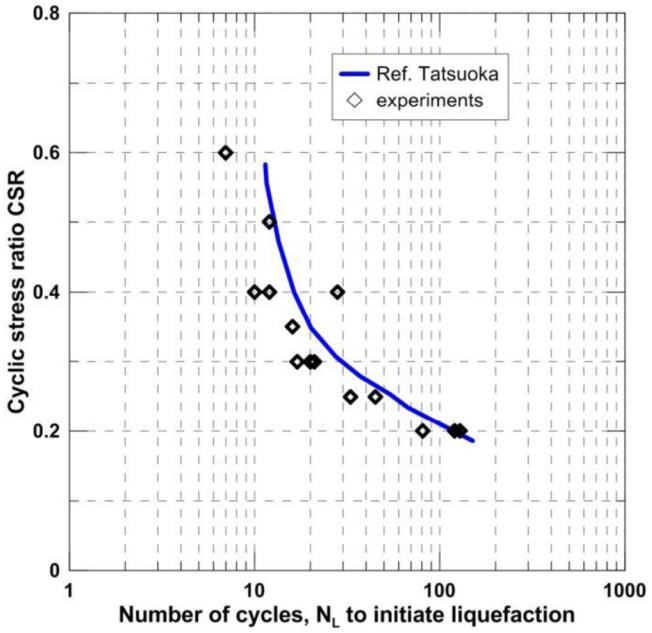

Fig. 12. Comparison of experimental results.

to better numerical simulation. The results obtained using the newly developed coupled model are closer to the experimental results. However, in simulation of pore pressures as the strain values increase the pore pressure is overestimated since the discretization of pore pressures is done by linear functions as shown in Fig. 2.

5.3.2. Simulation of dynamic – cyclic triaxial experiments

In order to simulate cyclic triaxial tests, the hypoplastic material model was extended by introducing the intergranular strain concept as explained in the work of Niemunis and Herle [41]. The constitutive equation used for the solid state in the multiphase model is hypoplastic material model as given in Eq. (55). The hypoplastic parameters of the Toyoura sand were added five more parameters in order to consider the accumulation of the strain due to cyclic loadings. Calibration of the parameters was done in the PhD work of the first author [36]. In Table 5, the extended hypoplastic parameters for the Toyoura sand are presented.

Cyclic triaxial tests were carried out to investigate the stress strain relations in different cycles. Own results were compared with the experimental results given in the work of Tatsuoka [47]. Undrained cyclic triaxial tests were carried out to determine the correctness of the performed tests in the laboratory. Cyclic triaxial tests were performed on the Toyoura sand samples that were saturated and consolidated before application of dynamic loading. The test data were analyzed considering the displacement and stress values for each cycle. In this study, the density of each layer was controlled by adjusting the number of tamping blows with a constant free fall of 2 cm. This method was adopted as simulation of field compaction of moist sand in layers by vertical tamping on the ground surface. After being saturated, each test specimen was consolidated isotropically. It was confirmed that the Skempton's B value had to be bigger than 0.95. The cyclic triaxial test results were normalized using the conventional stress ratio SR = $\sigma_{dp}/2\sigma_c'$, in which σ_{dp} is the maximum single amplitude of cyclic deviatoric stress and σ_c' is the effective isotropic consolidation stress. It should be stated that σ_{dp} is defined as the single amplitude cyclic axial load divided by the cross sectional area of the sample. The cyclic undrained triaxial strength was defined as 5%

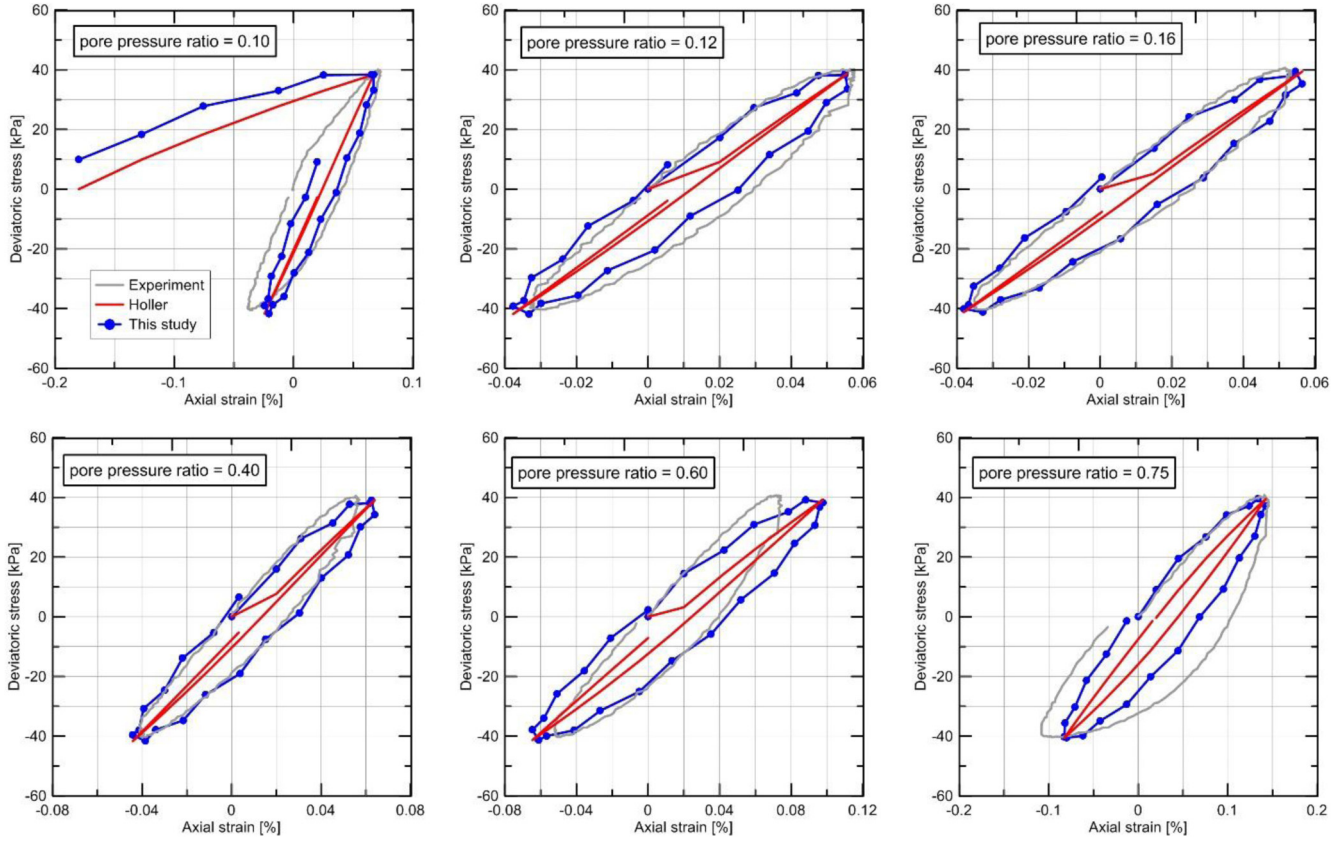

Fig. 13. Comparison between numerical and experimental values of deviatoric stress of cyclic stress ratio CSR 0.2 for different pore pressure ratios Δu.

Please cite this article in press as: Edip K et al. Development of coupled numerical model for simulation of multiphase soil. Comput Geotech (2017), https://doi.org/10.1016/j.compgeo.2017.08.016

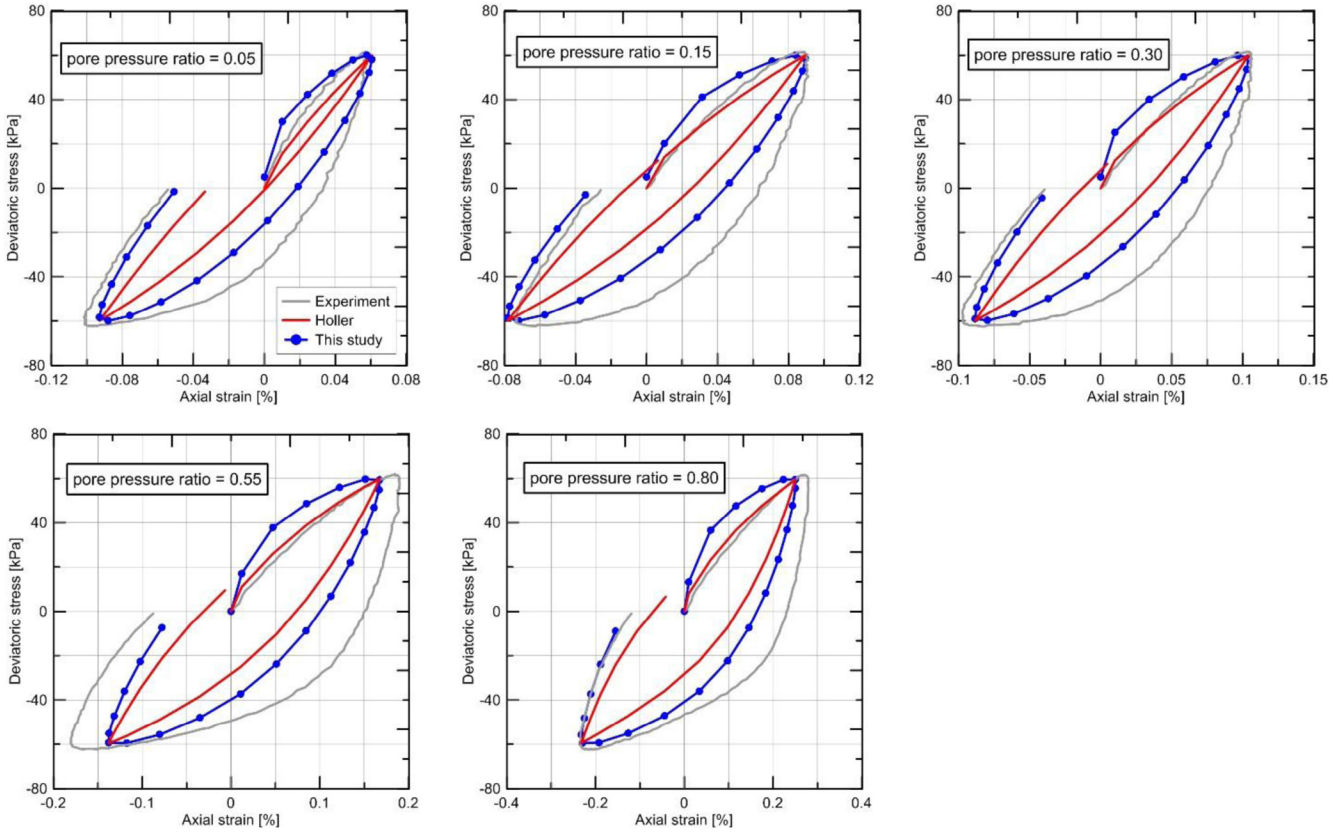

Fig. 14. Comparison between numerical and experimental values of deviatoric stress of cyclic stress ratio CSR = 0.3 for different pore pressure ratios Δu.

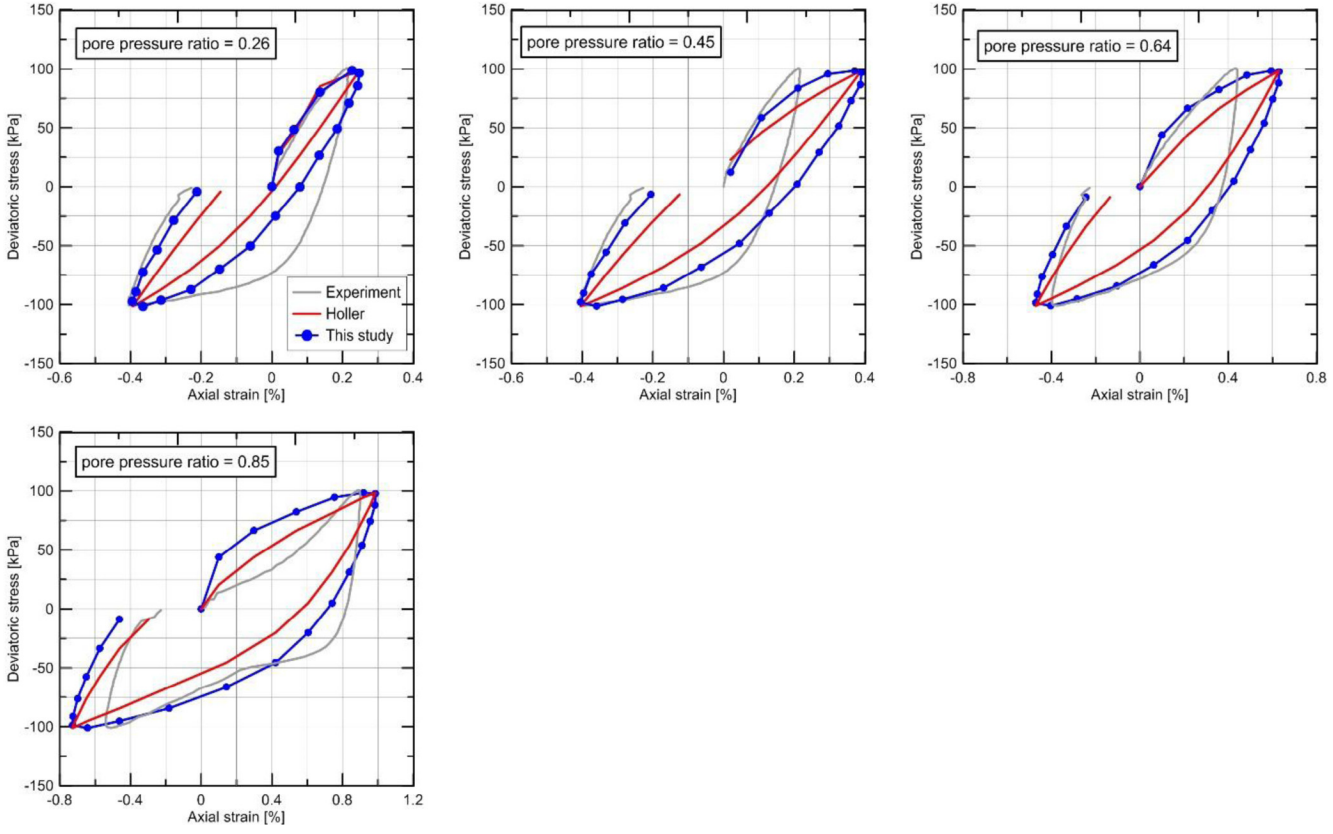

Fig. 15. Comparison between numerical and experimental results of deviatoric stress of cyclic stress ratio CSR = 0.5 for different pore pressure ratios.

Please cite this article in press as: Edip K et al. Development of coupled numerical model for simulation of multiphase soil. Comput Geotech (2017), https://doi.org/10.1016/j.compgeo.2017.08.016

double amplitude axial strain values. Thus the development of pore pressure to the value of confining pressure was not a criterion in the initiation of the liquefaction. It was found that the stress difference in cyclic tests had an effect of liquefaction initiation. The samples were reconstituted in dense state with an initial density of 75%. In total, fourteen cyclic triaxial tests were carried out on saturated and consolidated samples of identical size. The samples were pressurized with an effective mean pressure of p = 100 kPa. The cyclic loading stage was executed with user defined loading parameters under consolidated undrained conditions. Sinusoidal loading in compression and extension with a loading frequency of 0.5 Hz is applied to determine the number of cycles necessary to initiate the liquefaction.

The data from the cyclic triaxial tests show that the cyclic stress ratio and number of cycles causing the initial liquefaction is in accordance with curve found in the work of Tatsuoka [47]. In Fig. 12 the cyclic stress ratio versus the number of cycles is plotted for 5% double amplitude strain. All these data were used to obtain an information on the correctness of the experimental procedure at the Laboratory for Soil Testing (IZIIS-Skopje).

Three sets of experiments with cyclic stress ratio (CSR) of 0.2, 0.3 and 0.5 are presented and numerically simulated using the coupled model. The comparison of the numerical and experimental results shows a promising accordance. As can be seen from Figs. 13–15, the beginning and the mid values of the numerical simulation show a good agreement with each other. However, as the number of cycles increases the difference between the loops of numerical and experimental values increases. The main reason for this deviation is in the material model since only the smaller deformations are considered.

As it is seen in Fig. 13 the comparison of stress and strain values considering the cyclic stress ratio of small values enables a good correlation between numerical and experimental values. The numerical simulation using the newly developed coupled model gives acceptable results both at end values and in the mid values of the cycles.

From a constitutive modeling point of view, the newly developed coupled model proves to capture the material response quite well when small up to medium pore pressures are considered. As pore pressure increases the simulation results deviate from the experimental values.

From Figs. 13–15 it can be stated that the newly developed multiphase model estimates the stress values more realistically when compared with the model of Holler [27]. Although the end values at the graphs are almost the same, the middle steps using the newly developed coupled model seem to give better correspondence with the experimental values. Nevertheless, as strain increments increase the gap between numerical and experimental results increase which gives the possible points for further research in simulation.

6. Conclusion

In the present paper, a numerical model is presented for analysis of multiphase porous media in which both solid deformation and flow of liquid phases under isothermal conditions takes part.

The coupling of solid and fluid phases is considered taking into account the fluid compressibilites and permeabilities. Two benchmark problems are selected to prove the accuracy of the proposed model such as drainage and partially saturation problems. Numerical simulations of seepage and partial consolidation give similar results with the experimental and other results from reference works.

The application of the proposed model is verified through computation of triaxial experiments in which the solid state of the proposed model is simulated using a nonlinear hypoplastic model. In cyclic triaxial experiments, the hypoplastic model is extended in order to consider the intergranular strain in cyclic loadings. The comparative study makes it obvious that the proposed model is reliable for predicting the response of both static and dynamic loadings when small deformations are considered.

Acknowledgments

Financial support of the Herder Foundation and the German Academic Exchange Service (DAAD) is gratefully acknowledged. Special thanks to em. Prof. Dr. Guenther Schmid, PhD for his advice and support.

References

[1] De Boer R. Development of porous media theories—a brief historical review. Transp Porous Media 1992;9(1–2):155–64.
[2] Terzaghi K. Theoretical soil mechanics; 1943.
[3] Biot MA. General theory of three-dimensional consolidation. J Appl Phys 1941;12(2):155–64.
[4] Biot M. Generalized theory of acoustic propagation in porous dissipative media. J Acoust Soc Am 1962;34:1254.
[5] Morland L. A simple constitutive theory for a fluid-saturated porous solid. J Geophys Res 1972;77(5):890–900.
[6] Goodman M, Cowin S. A continuum theory for granular materials. Arch Ration Mech Anal 1972;44(4):249–66.
[7] Sampaio R. An axiomatic theory of mixtures with diffusion. Arch Ration Mech Anal 1976;62(2):99–116.
[8] Bowen RM. Incompressible porous media models by use of the theory of mixtures. Int J Eng Sci 1980;18(9):1129–48.
[9] Bowen RM. Compressible porous media models by use of the theory of mixtures. Int J Eng Sci 1982;20(6):697–735.
[10] Whitaker S. Flow in porous media II: The governing equations for immiscible, two-phase flow. Transp Porous Media 1986;1(2):105–25.
[11] Whitaker S. Flow in porous media I: a theoretical derivation of Darcy's law. Transp Porous Media 1986;1(1):3–25.
[12] Hassanizadeh M, Gray WG. General conservation equations for multi-phase systems: 1. Averaging procedure. Adv Water Resour 1979;2:131–44.
[13] Hassanizadeh M, Gray WG. General conservation equations for multiphase systems: 2. Mass, momenta, energy, and entropy equations. Adv Water Resour 1979;2(4):191–203.
[14] Hassanizadeh M, Gray WG. General conservation equations for multi-phase systems: 3. Constitutive theory for porous media flow. Adv Water Resour 1980;3(1):25–40.
[15] Fredlund DG, Morgenstern NR. Stress state variables for unsaturated soils. J Geotech Geoenviron Eng 1977 103(ASCE 12919).
[16] Chang C, Duncan J. Consolidation analysis for partly saturated clay by using an elastic–plastic effective stress–strain model. Int J Numer Anal Meth Geomech 1983;7(1):39–55.
[17] De Boer R, Kowalski SJ. A plasticity theory for fluid-saturated porous solids. Int J Eng Sci 1983;21(11):1343–57.
[18] Zienkiewicz OC, et al. Static and dynamic behaviour of soils: a rational approach to quantitative solutions. II. Semi-saturated problems. Proceedings of the Royal Society of London. A. Mathematical and Physical Sciences 1990:429(1877);311–21.
[19] Zienkiewicz OC, et al., Static and dynamic behaviour of soils: a rational approach to quantitative solutions. I. Fully saturated problems. Proc Roy Soc Lond A. Math Phys Sci 1990;429(1877):285–309.
[20] Alonso EAPdA, Gens Solé A, Josa Garcia-Tornel A. A constitutive model for partially saturated soils; 2011.
[21] Schrefler BA, Zhan X, Simoni L. A coupled model for water flow, airflow and heat flow in deformable porous media. Int J Numer Meth Heat Fluid Flow 1995;5(6):531–47.
[22] Gawin D, Baggio P, Schrefler BA. Coupled heat, water and gas flow in deformable porous media. Int J Numer Meth Fluids 1995;20(8–9):969–87.
[23] Lewis RW, Schrefler BA. The finite element method in the static and dynamic deformation and consolidation of porous media. 2nd ed. Wiley Verlag; 1998.
[24] Schrefler BA, Scotta R. A fully coupled dynamic model for two-phase fluid flow in deformable porous media. Comput Methods Appl Mech Eng 2001;190(24–25):3223–46.
[25] Wieners C et al. Parallel 3-d simulations for porous media models in soil mechanics. Comput Mech 2002;29(1):75–87.
[26] Oettl G. A three-phase FE-model for dewatering of soils by means of compressed air. Universitaet Innsbruck; 2003.
[27] Stefan H. Dynamisches Mehrphasenmodell mit hypoplastischer Materialformulierung der Feststoffphase. Germany: RWTH Aachen University; 2006.
[28] Liakopoulos AC. Transient flow through unsaturated porous media. Berkeley: University of California; 1965.

[29] Khoei AR, Mohammadnejad T. Numerical modeling of multiphase fluid flow in deforming porous media: a comparison between two- and three-phase models for seismic analysis of earth and rockfill dams. Comput Geotech 2011;38(2):142–66.
[30] Bedford A, Drumheller DS. Theories of immiscible and structured mixtures. Int J Eng Sci 1983;21(8):863–960.
[31] de Boer IR, Ehlers IW. A historical review of the formulation of porous media theories. Acta Mech 1988;74(1–4):1–8.
[32] Ehlers W, Volk W. On theoretical and numerical methods in the theory of porous media based on polar and non-polar elasto-plastic solid materials. Int J Solids Struct 1998;35(34):4597–617.
[33] Ricken T, de Boer R. Multiphase flow in a capillary porous medium. Comput Mater Sci 2003;28(3–4):704–13.
[34] Bishop A. The effective stress principle. Teknisk Ukeblad 1959;39:859–63.
[35] Biot MA, Willis DG. The elastic coefficients of the theory of consolidation. J Appl Mech 1957;24(4):594–601.
[36] Edip K. Development of three phase model with finite and infinite elements for dynamic analysis of soil media, 2013, Ss. Cyril and Methodius: Institute of Earthquake Engineering and Engineering Seismology.
[37] ANSYS. Fem Software; 2006.
[38] von Wolffersdorff PA. A hypoplastic relation for granular materials with a predefined limit state surface. Mech Cohesive-frictional Mater 1996;1(3):251–71.
[39] Wu W, Bauer E, Kolymbas D. Hypoplastic constitutive model with critical state for granular materials. Mech Mater 1996;23(1):45–69.
[40] Herle I, Gudehus G. Determination of parameters of a hypoplastic constitutive model from properties of grain assemblies. Mech Cohesive-frictional Mater 1999;4(5):461–86.
[41] Niemunis A, Herle I. Hypoplastic model for cohesionless soils with elastic strain range. Mech Cohesive-frictional Mater 1997;2(4):279–99.
[42] Laloui L, Klubertanz G, Vulliet L. Solid–liquid–air coupling in multiphase porous media. Int J Numer Anal Meth Geomech 2003;27(3):183–206.
[43] Khoei A, Haghighat E. Extended finite element modeling of deformable porous media with arbitrary interfaces. Appl Math Model 2011;35(11):5426–41.
[44] Brooks RN, Corey AT. Properties of porous media affecting fluid flow. J Irrigat Drain Div Am Soc Civil Eng 1966;92:61–68.
[45] Herle I. Hypoplastizität und Granulometrie einfacher Korngerüste, 1997: Inst. für Bodenmech. u. Felsmech. der Universität Fridericiana in Karlsruhe, Heft 142.
[46] Herle I. Hypoplastizität und Granulometrie einfacher Korngerüste. Vol. 142. Inst. für Bodenmechanik und Felsmechanik der Univ. Fridericiana; 1997.
[47] Tatsuoka F et al. Cyclic undrained triaxial and torsional shear strength of sands for different sample preparation methods. Soils Found 1986;26(3):23–41.

Please cite this article in press as: Edip K et al. Development of coupled numerical model for simulation of multiphase soil. Comput Geotech (2017), https://doi.org/10.1016/j.compgeo.2017.08.016